Available online at www.sciencedirect.com
ScienceDirect
Catalysis Today 119 (2007) 137–144
CATALYSIS TODAY
www.elsevier.com/locate/cattod

Characterization and catalytic investigation of Fe-ZSM5 for urea-SCR

Mukundan Devadas [a], Oliver Kröcher [a,*], Martin Elsener [a], Alexander Wokaun [a], George Mitrikas [b], Nicola Söger [c], Marcus Pfeifer [c], Yvonne Demel [c], Lothar Mussmann [c]

[a] *Paul Scherrer Institute, CH-5232 Villigen PSI, Switzerland*
[b] *Physical Chemistry Laboratory, Swiss Federal Institute of Technology (ETHZ) Zurich, Wolfgang-Pauli Str. 10, CH-8093 Zurich, Switzerland*
[c] *Umicore AG & Co. KG, Automotive Catalysts, Rodenbacher Chaussee 4, D-63403 Hanau, Germany*

Available online 11 September 2006

Abstract

Fe-ZSM5 was prepared with high iron content by solid-state ion exchange and characterized by ICP-AES, BET surface measurements, TEM, UV–vis, EPR and DRIFT spectroscopy as well as supplementing catalytic tests in order to clear up its functionality in urea-SCR. Due to the over-exchange with iron small Fe_2O_3 particles were formed, identified by UV–vis, EPR and TEM measurements, which were proved to be not active for the SCR reaction. However, the oxidation of NO to NO_2 over Fe^{3+} ions in the catalyst was realized to be a pre-requisite for the SCR reaction and the rate-determining step. DRIFT investigations under SCR conditions showed adsorbates on Fe^{2+} up to 300 °C. The high SCR activity above 300 °C can be explained by the faster reoxidation of Fe^{2+} to Fe^{3+} sites at high temperatures. The observed inhibition of the SCR reaction by excess ammonia at low and intermediate temperatures can be explained in this context by the reducing properties of ammonia converting Fe^{3+} to Fe^{2+} or by preventing the reoxidation of Fe^{2+}.

Keywords: Fe-ZSM5; Ammonia; SCR; Monolith; EPR; DRIFT; Ammonia inhibition

1. Introduction

Fe-ZSM5 has gained much attention as active and stable catalyst for the selective catalytic reduction of NO_x emissions from diesel engines with urea (urea-SCR) [1–5]. As urea needs to be decomposed to ammonia in the SCR process, ammonia is a suitable substitute in laboratory investigations of the SCR process [1]. For NO the SCR reaction is described by the following reaction equation (standard SCR):

$$4NH_3 + 4NO + O_2 \rightarrow 4N_2 + 6H_2O \quad (1)$$

The aim of the study was to characterize Fe-ZSM5 under *ex situ* and *in situ* conditions in order to understand the functionality of this catalyst in NH_3-SCR. Some investigations have already been made with a similar objective, but the present work is focused on Fe-ZSM5 samples with optimized SCR activity similar to those to be used in real SCR systems onboard of diesel vehicles. In preliminary tests three different preparation methods for Fe-ZSM5 have been tested: wet ion exchange, a so-called ''mechanochemical'' method [6] and solid-state ion exchange. As expected, solid-state ion exchange yielded the most active SCR catalyst [7]. Due to the high activity of Fe-ZSM5 prepared by this method and the suitability of this method for a large scale production it is also applied for the industrial production process [7]. However, the main drawback of the method for structural investigations is that it usually results in over-exchanged Fe-ZSM5 with various iron species, which complicates the investigation of the catalyst functionality. Nevertheless, since we aimed at information useful for the real-world application of Fe-ZSM5 we focused particularly on Fe-ZSM5 prepared by solid-state ion exchange. The catalytic activity of the material used in this work has

* Corresponding author. Tel.: +41 56 310 20 66; fax: +41 56 310 23 23.
E-mail address: oliver.kroecher@psi.ch (O. Kröcher).

0920-5861/$ – see front matter © 2006 Elsevier B.V. All rights reserved.
doi:10.1016/j.cattod.2006.08.018

already been published in [8]. However, supplementing catalytic tests were performed with Fe-ZSM5 and the base-material H-ZSM5 for a better understanding of the mechanism. The zeolite powders were coated on monolith supports, which allowed us to test the catalytic performance of the materials similar to the conditions at the diesel engine.

2. Experimental

2.1. Catalyst preparation

Fe-ZSM5 was prepared by solid-state ion exchange. The base material H-ZSM5, supplied by Umicore AG, was added to iron(II) chloride in the weight ratio 2:1 and mixed in a ball mill for 1 h. The resulting powder was calcined at 550 °C for 5 h. After calcination, the material was washed with deionised water until all chloride ions have been removed, which was tested with silver nitrate solution. Finally the sample was dried at 100 °C for 10 h. The Fe-ZSM5 obtained as well as the base material H-ZSM5 were coated on cordierite monoliths with a cell density of 400 cpsi by the procedure described in [8]. The active mass loaded on the monolith is 0.82 g (Fe-ZSM5) and 0.80 g (H-ZSM5).

2.2. Catalyst characterization

Inductively coupled plasma-atomic emission spectroscopy (ICP-AES) was used for the quantitative analysis of the elemental composition of the sample. The instrument was a Varian Vista AX spectrometer. The sample was dissolved in a mixture of 1 ml HF, 0.5 ml HCl, 2.5 ml HNO_3 and 10 ml H_2O. Then the mixture was placed in a water bath at 95 °C for 3 h. For analysis, H_3BO_3 was added to 1 ml of the dissolved mixture and filled up to 25 ml with water. A Micromeritics ASAP 2000 analyzer was used to measure the N_2 adsorption isotherms of the sample. Prior to the experiment the sample was pretreated overnight under vacuum at 250 °C.

Transmission electron microscopy (TEM) measurements were performed on a JEOL 2010 microscope equipped with a LaB_6 cathode and with high-tilt objective lenses. The acceleration voltage was 200 kV.

A diffuse reflectance UV–vis spectrum of the catalyst was measured on a Cary 400UV-Vis spectrometer equipped with a Praying Mantis sample stage from Harrick. $BaSO_4$ was used as Ref.

Electron paramagnetic resonance (EPR) measurements have been carried out using an ELEXYS Bruker spectrometer (X-band microwave frequency), at temperatures 20 and −150 °C.

Diffuse reflectance infrared Fourier transform (DRIFT) spectra were recorded with a Nexus 860 Thermo Nicolet spectrometer in a DRIFT cell equipped with ZnSe windows. The sample was pre-treated at 450 °C for 1 h in flowing N_2. At each temperature the background spectrum was recorded and subtracted from the sample spectrum obtained at the same temperature. In the experiment the IR spectra were recorded at 200 scans at a spectral resolution of 4 cm^{-1}. The total gas flow entering the cell was 40 ml/min.

2.3. Activity measurements

The setup of the test apparatus used to measure the NO_x conversion ($DeNO_x$) has been described in [9]. The composition of diesel exhaust gas was approximated by a model feed gas containing 10% O_2, 5% H_2O, 1000 ppm of NO and balance N_2. NH_3 was added in the range 100–1000 ppm. The gas hourly space velocity (GHSV = volumetric gas flow/coated monolith volume) was 52,000 h^{-1}. The NO oxidation capacity of H-ZSM5 and Fe-ZSM5 was investigated at the same GHSV with a feed gas composed of 10% O_2, 5% H_2O, balance N_2 and 1000 ppm NO.

3. Results

3.1. ICP-AES and low temperature N_2 adsorption

The micropore volume and elemental composition of Fe-ZSM5 and H-ZSM5 are shown in Table 1. After ion exchange and calcination treatments, the micropore volume decreased from 0.11 to 0.08 cm^3/g, respectively. The Si/Al ratio remained the same. The amount of Fe which got loaded into the zeolite is 11.4 wt.%. The XRD patterns of Fe-ZSM5 and the parent H-ZSM5 are plotted in [8]. The MFI structure of the parent H-ZSM5 was maintained in Fe-ZSM5 after solid-state ion exchange and calcinations, but the additional formation of Fe_2O_3 in the hematite phase was observed.

3.2. TEM

Fig. 1 shows two TEM pictures of the Fe-ZSM5 sample. The presence of small (Fig. 1A) and large dark spots (Fig. 1B) were observed. These black spots of 20–50 nm size are attributed to Fe_2O_3 particles, which is supported by the XRD results.

3.3. UV–vis

Fig. 2 shows the UV–vis spectrum of Fe-ZSM5. Most dominant is the strong band at around 35,000 cm^{-1}, accompanied with a shoulder around 45,000 cm^{-1}. In addition a band around 15,000 cm^{-1} and a strong absorption edge around 18,400 cm^{-1} were formed. Shoulders around 20,000 and 28,000 cm^{-1} were also observed.

For Fe^{3+} two ligand-to-metal charge transfer (CT) transitions, $t_1 \rightarrow t_2$ and $t_1 \rightarrow e$, are expected [10]. The bands at 35,000 cm^{-1} and 45,000 cm^{-1} are attributed to isolated Fe^{3+} sites at octahedral and tetrahedral positions, respectively [11]. The low intensity band at 15,000 cm^{-1} and the absorption edge

Table 1
Low temperature N_2 adsorption and ICP-AES results

	Micropore volume (cm^3/g)[a]	Si/Al[b]	Fe/Al[b]	Fe (wt.%)[b]
Fe-ZSM5	0.081	28	2.3	11.4
H-ZSM5	0.111	28	–	–

[a] Determined from low temperature nitrogen adsorption analysis.
[b] Determined from ICP-AES analysis.

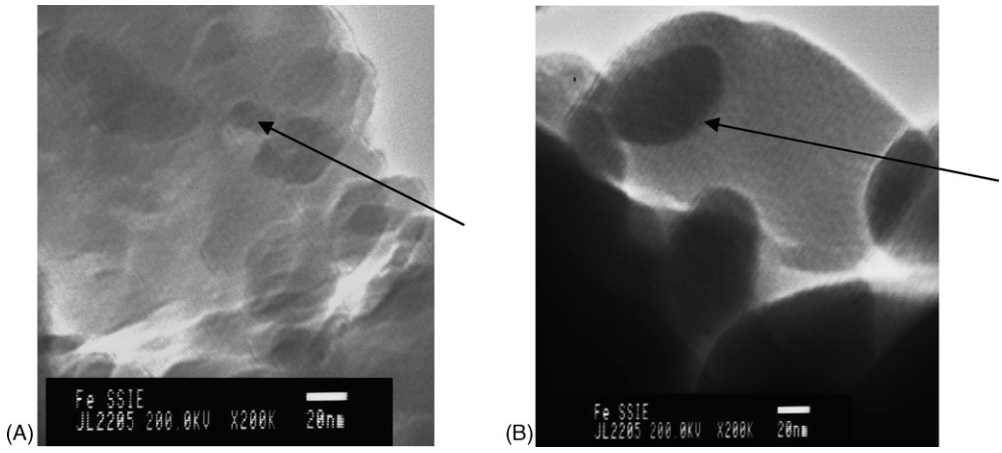

Fig. 1. TEM micrographs of Fe-ZSM5.

around 18,400 cm^{-1} are assigned to Fe oxide like species. The strong absorption edge at 18,400 cm^{-1} corresponds to the d–d electron pair transition (EPT), which is unique for the presence of Fe^{3+} in Fe_2O_3 (hematite) [12,13]. The position of the EPT band depends on the particle size of hematite [12]. From the EPT band in the range 18,200–18,900 cm^{-1} a hematite particle size of about 10–50 nm is derived, which confirms the results of the TEM analysis. For highly loaded Fe-MFI, the bands around 20,000 cm^{-1} are ascribed to Fe_2O_3 particles [14]. The shoulder at 28,000 cm^{-1} is characteristic for iron oxo dimmers, such as $[HO–Fe-O–Fe–OH]^{2+}$, which are bound to the zeolite framework via iron oxygen bridges [15].

3.4. EPR spectroscopy

The results of the EPR measurements are shown in Fig. 3. The spectra consist of signals in two regions, i.e. signals at $g \geq 4.2$ and signals at $g \geq 2.0$. In the region at $g \geq 4.2$ there is a main signal at $g \sim 4.27$ and others less intense at $g \sim 5.6$ and 8.5. The intensity of the signals at $g \geq 4.2$ increases with decreasing temperature. A second group of signals is located in the zone $g \sim 2.0$, for both spectra. At −150 °C, the signal at $g \sim 2.3$ is decreased in intensity and the signal at $g \sim 2.3$ is shifted to lower magnetic fields. A strong peak is observed at $g \sim 2$.

The observed signals are common for Fe-ZSM5 zeolites [16,17] and also for Fe^{3+} ions in other oxide matrices. The number and positions of EPR transitions for Fe^{3+} ions observable in a powder spectrum depend sensitively on the local crystal powder spectrum of these sites and possible magnetic interactions between them. Goldfarb et al. [17] attributed the signals at $g \sim 4.3$ and $g \geq 6$ to arise from $|-1/2> \leftrightarrow >1/2|$ transition of isolated Fe^{3+} sites in strong rhombic or axial distortion. Based on [17], Kumar et al. [18] implied that an Fe^{3+} species giving rise to a line at $g \sim 4.3$ is more strongly distorted than an Fe^{3+} site represented by a signal at $g \sim 6$ due to the difference in the magnitude of E. The signal at $g \sim 4.3$ is assigned to Fe^{3+} sites incorporated in tetrahedral positions while the line at $g \sim 6$ is assigned to isolated Fe^{3+} species in higher coordination numbers [17]. Signals at $g \sim 2$ can arise from isolated Fe^{3+} or from Fe_xO_y clusters. The broad line at $g = 2.3$ is attributed to small Fe_2O_3 particles [17]. The signal at $g \sim 2.3$ disappear at −150 °C and do not follow the paramagnetic behaviour, indicating that the corresponding Fe^{3+} ions are in mutual magnetic interaction. The sharp signal at $g \sim 2$ at −150 °C was also observed by Chen et al. [19], who assigned the peak to superoxide ions (O_2^-) which are associated with iron ions.

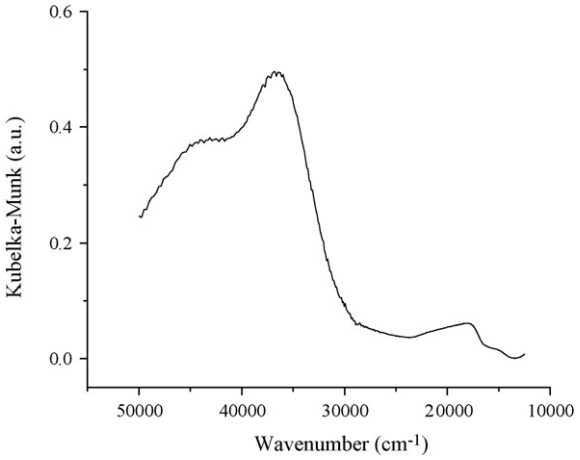

Fig. 2. UV–vis spectrum of Fe-ZSM5.

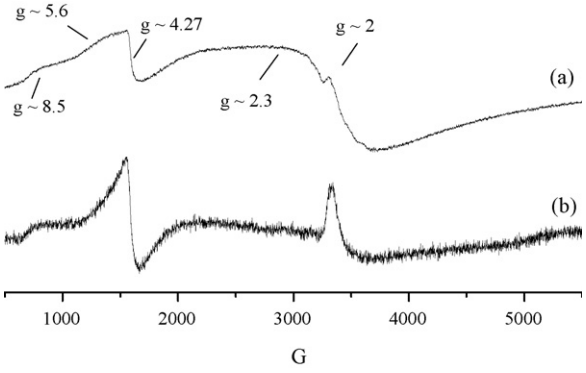

Fig. 3. EPR spectra of Fe-ZSM5 at (a) 20 °C and (b) −150 °C.

3.5. DRIFT spectroscopy

Fig. 4 shows the spectra on adsorption of NO, NO_2 and $NO + O_2$ for 30 min at 35 °C, followed by purging with nitrogen for 60 min at the same temperature. Adsorption of NO leads to the formation of bands at three positions (Fig. 4a). The band at 1880 cm^{-1} has been assigned to mono-nitrosylic species associated with Fe sites in the 2+ state (Fe^{2+}-NO) [20]. In addition to this band, a shoulder at 1815 cm^{-1} is observed. This shoulder is assigned to species bound to Fe-oxide ions. The band at 2140 cm^{-1} is attributed to NO^+ attached to Brønsted acid sites [21]. Introduction of NO at 35 °C, resulted in a strong decrease in intensity of the band at 3605 cm^{-1} (not shown here), which is attributed to the formation of NO^+ species on ion exchange positions.

On NO_2 adsorption (Fig. 4b), the same band appears at 2140 cm^{-1} as reported for the NO treatment (Fig. 4a). Apart from that, bands at 1635, 1578 cm^{-1} and a shoulder at 1605 cm^{-1} were observed. The band at 1635 cm^{-1} is assigned to adsorbed NO_2 species [21] and the bands at 1578 cm^{-1} and 1605 are assigned to nitrate species [22]. In the presence of $NO + O_2$ (Fig. 4c), the bands at 1635, 1605 and 1578 cm^{-1} characteristic for adsorbed NO_2 and nitrates occur again.

The reaction between NO adspecies and NH_3 was also followed by DRIFT measurements (Fig. 5). A temperature of only 100 °C was chosen in order to reduce the reaction rate, whereby the concentration of surface species was enhanced to a detectable level. First, Fe-ZSM5 was treated with 500 ppm NO for 30 min at 100 °C (Fig. 5A(a)). After stopping the NO dosage, NH_3 (500 ppm) was introduced and the spectra were recorded as function of time (Fig. 5A(b–e)). Finally, the NH_3 dosage was stopped and the catalyst was purged with N_2 for 30 min (Fig. 5A(f)). It is clearly discernible, that bands at 3374 and 3282 cm^{-1} are emerging when NH_3 is adsorbed on the catalysts and that these bands are stable after purging with N_2. The bands are assigned to NH_4^+ ions with three hydrogen atoms bonded to three oxygen ions of AlO_4 tetrahedra (3H structure).

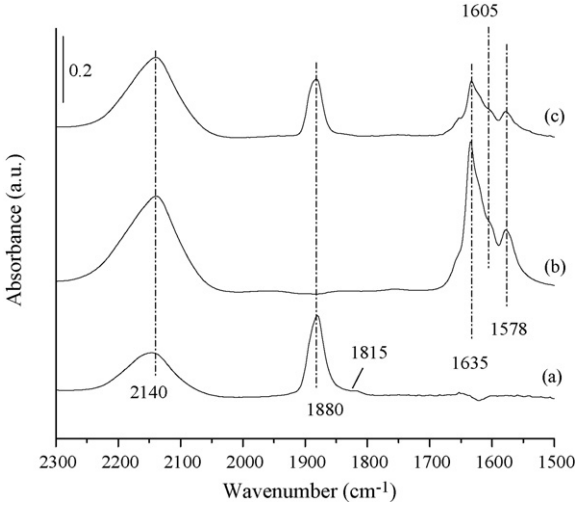

Fig. 4. FT-IR spectra of Fe-ZSM5 treated with (a) 500 ppm NO, (b) 500 ppm NO_2, and (c) 500 ppm NO + 5% O_2 at 35 °C for 30 min followed by purging with nitrogen for 60 min.

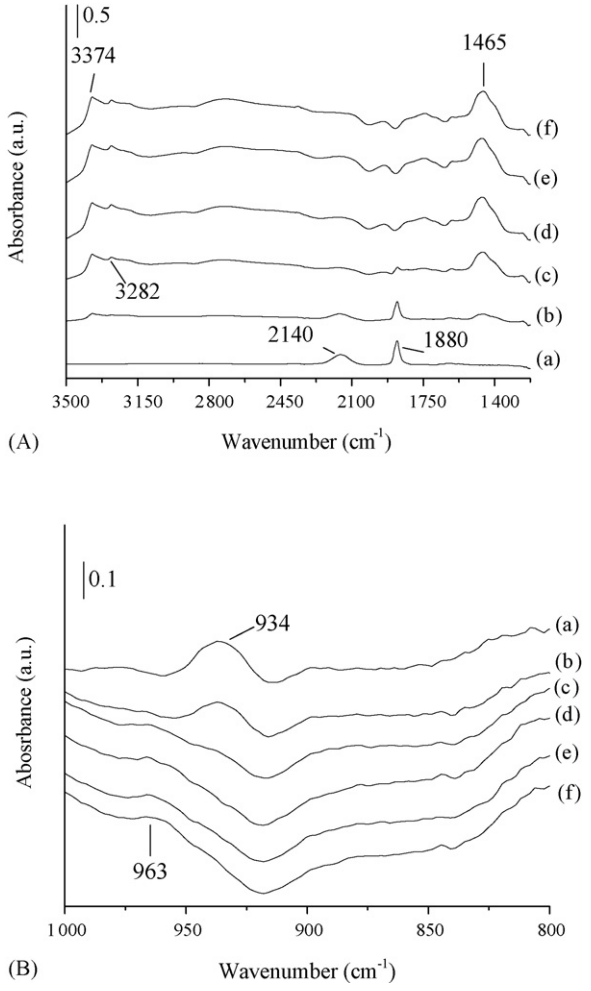

Fig. 5. (A) FT-IR spectra of Fe-ZSM5 at 100 °C during reaction between NH_3 and pre-adsorbed NO. (a) After NO adsorption, (b) after NH_3 dosage for 2 min, (c) 5 min, (d) 10 min, (e) 15 min, and (f) after NH_3 dosing and purging with N_2 for 30 min. (B) FT-IR spectra of the T–O–T region of Fe-ZSM5 at 100 °C during reaction between NH_3 and pre-adsorbed NO. (a) After NO adsorption, (b) after NH_3 dosage for 2 min, (c) 5 min, (d) 10 min, (e) 15 min, and (f) after NH_3 dosing and purging with N_2 for 30 min.

Weaker bands at 3180 and 2925 cm^{-1} are attributed to NH_4^+ ions with two hydrogen atoms bonded to AlO_4 tetrahedra (2H structure) [23,24]. The band at 1465 cm^{-1}, which was also observed with increasing NH_3 flow, is due to the asymmetric bending vibration of NH_4^+ chemisorbed on Brønsted acid sites [25]. Concurrently, the bands at 2140 and 1880 cm^{-1} disappeared within 5 min of NH_3 flow indicating the reaction of pre-adsorbed NO with NH_3. The band at 934 cm^{-1} which arise due to NO interaction with Fe-ZSM5 is typical for iron ions located in cationic sites (Fig. 5B(a)) [26]. On passing NH_3, the 934 cm^{-1} band started to disappear and a broad band centred at 963 cm^{-1} was formed (Fig. 5B(b–e)). This broad band is assumed to be associated with the T–O–T band perturbed by Fe^{2+} species [27], most likely by $[Fe(NH_3)_n]^{2+}$ with $n = 0$, 1 or 2. The same pattern was also observed for the T–O–T vibration region when NH_3 was dosed after pre-treatment with $NO + O_2$. Therefore, the appearance of the 963 cm^{-1} band ($[Fe(NH_3)_n]^{2+}$) in combination with the

concurrent disappearance of the 1880 cm^{-1} band (Fe^{2+}-NO) indicate that Fe is significantly in the 2+ state at lower temperatures on NO and NH_3 treatment.

In order to observe the changes in surface species at higher temperatures also spectra at 200, 300 and 400 °C were recorded (Fig. 6). Fig. 6A clearly shows that NH_4^+ ions with 3H and 2H structures are present on the surface of Fe-ZSM5 up to 300 °C during reaction conditions.

3.6. Catalytic testing

The NO_x reduction efficiency ($DeNO_x$) and functionality of the catalysts have been investigated with model gases at standard exhaust conditions. In Fig. 7 the $DeNO_x$ values are plotted versus the inlet NH_3 concentration for the Fe-ZSM5 monolith catalyst. For temperatures above 350 °C the $DeNO_x$ values increased with increasing ammonia concentration as expected. For lower temperatures, NO_x conversion first increases with increasing NH_3 concentration as expected, but then decreases if ammonia is overdosed and ammonia slip is forced. This means that the SCR reaction is inhibited by ammonia. This ammonia inhibition effect increases with decreasing temperatures.

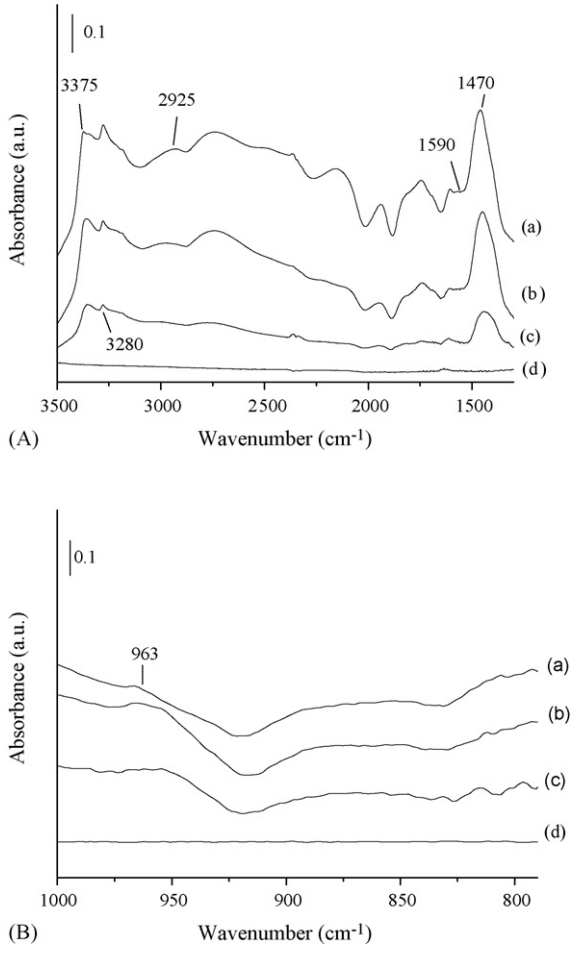

Fig. 6. (A) FT-IR spectra of Fe-ZSM5 after 30 min of reaction in a flow of 500 ppm NO, 10% O_2, and 500 ppm NH_3 in nitrogen: (a) 100 °C, (b) 200 °C, (c) 300 °C and (d) 400 °C. (B) FT-IR spectra of the T–O–T region of Fe-ZSM5 after 30 min of reaction in a flow of 500 ppm NO, 10% O_2, and 500 ppm NH_3 in nitrogen: (a) 100 °C, (b) 200 °C, (c) 300 °C and (d) 400.

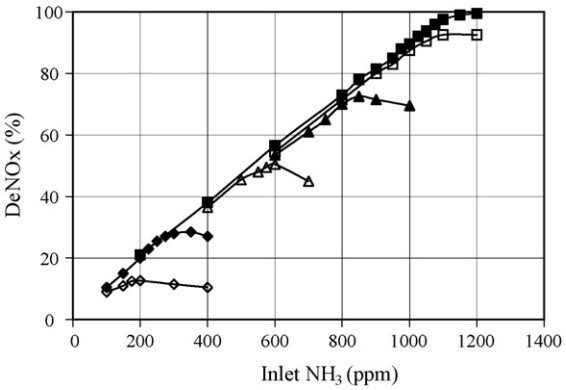

Fig. 7. $DeNO_x$ vs. inlet concentration of NH_3 for the fresh Fe-ZSM5 monolith catalyst at (◇) 200 °C, (◆) 250 °C, (△) 300 °C, (▲) 350 °C, (□) 400 °C and (■) 450 °C.

As mentioned in [1] ammonia emissions of about 10 ppm in average are regarded as harmless for automotive applications. Therefore, it is useful to express the temperature dependency of the catalyst activity by plotting the $DeNO_x$ values at 10 ppm ammonia slip independent of the NH_3/NO_x feed ratio. Fig. 8 shows this graph for H-ZSM5 and Fe-ZSM5 monolith catalysts. The corresponding ammonia concentrations in the feed are plotted in the same figure. For Fe-ZSM5, the $DeNO_x$ activity is steadily increasing from 200 to 450 °C, reaching ≥90% for $T \geq 400$ °C. The base material H-ZSM5 was nearly inactive for the SCR reaction, a $DeNO_x$ of max. 9% was achieved at $T \geq 400$ °C. For a Fe-ZSM5 sample prepared with the fortieth part of iron compared to the material in the present work, only a moderate decrease in $DeNO_x$ was observed, indicating that iron impurities in H-ZSM5 may be sufficient to cause its residual SCR activity. No N_2O could be detected for all catalysts over the entire temperature range. In Fig. 9 it is shown, that Fe-ZSM5 has a much higher NO oxidation capacity than H-ZSM5, which goes in parallel with the SCR activity of the two catalysts.

The presence of large amounts of Fe_2O_3 clusters in Fe-ZSM5 was observed by EPR and TEM measurements. In order to rule out that Fe_2O_3 is the active species in SCR, Fe_2O_3/MFI

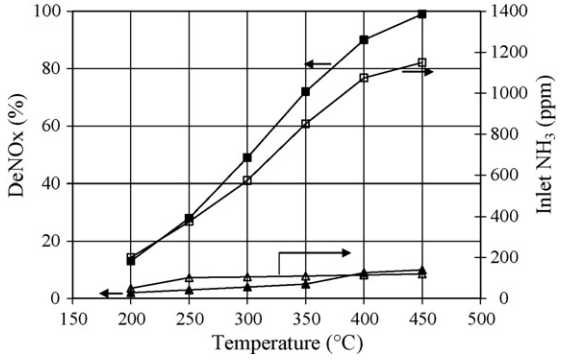

Fig. 8. $DeNO_x$ activity (closed symbol) and inlet ammonia (open symbol) of (■, □) Fe-ZSM5 and (▲, △) H-ZSM5 at 10 ppm NH_3 slip.

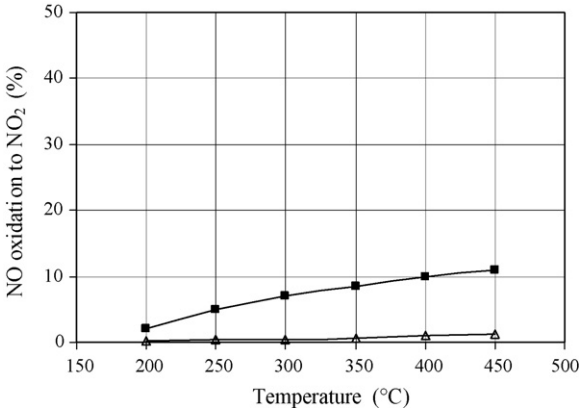

Fig. 9. NO oxidation capacity of (■) Fe-ZSM5 and (△) H-ZSM5.

was prepared as reference sample by incipient wetness impregnation and coated on a monolith. This catalyst was relatively inactive at high temperatures and completely inactive at lower temperatures (~20% $DeNO_x$ at $T \geq 400$ °C and ~10% at $T \geq 350$ °C). It was also observed the catalyst was nearly inactive for the oxidation of NO to NO_2 (~4% at $T \geq 400$ °C).

4. Discussion

The Fe-ZSM5 catalyst was prepared by solid-state ion exchange of H-ZSM5 with ferrous chloride in air, supporting the oxidation of the divalent iron to the trivalent state. ICP-AES results in a Fe/Al ratio of 2.3 for the catalyst implying that it is an ''over-exchanged'' zeolite (M/Al > 1). The nitrogen adsorption experiments evidenced a decrease of the pore volume by the ion exchange process, indicating that some of the pores are blocked, probably by the iron oxide particles detected by XRD and TEM. However, part of the particles might also be present on the outer surface of the zeolite crystals, not influencing the accessibility to the pores. It is plausible that during ion exchange small particles of $FeCl_2$ are nucleated within the pores of the zeolites, whose hydrolysis would lead the formation of FeO_x particles [28]. The other possibility for the formation of FeO_x might be the drying period in the presence of air:

$$FeCl_2 \cdot 4H_2O + \text{H-ZSM5} \xrightarrow{\text{air}/550\,^\circ\text{C}} \text{FeCl-ZSM5} + 4H_2O + HCl \quad (2)$$

$$2\text{FeCl-ZSM5} + H_2O \xrightarrow{\text{washing/drying}} \text{Fe-ZSM5-FeO}_x + 2HCl \quad (3)$$

From the many features found in the UV–vis spectrum isolated iron species in tetrahedral and octahedral environment, iron oxo dimers could be clearly identified. Iron oxide particles have also been detected in XRD and TEM investigations. The broad variety of iron species was confirmed by the EPR measurements, from which only the signal at $g \sim 2$ shall be emphasized, assigned by Chen et al. [19] to superoxide ions (O_2^-) which are associated with iron ions. This peak is very sensitive and disappears at temperatures above −150 °C as well as upon adsorption of H_2O or NH_3 [19]. However, the superoxide ions might be involved in the reaction at higher temperatures as a short lived reaction intermediate.

In the DRIFT spectra, a strong band at 2140 cm^{-1} was obtained on adsorption of NO on Fe-ZSM5. This band was also observed for the base material H-ZSM5 when NO was adsorbed (not shown here). The 1880 cm^{-1} band is often observed after NO adsorption on different Fe-exchanged zeolites [29,30] and oxide supported Fe^{n+} ions [31,32]. This band evolves in parallel with the NO^+ band at 2140 cm^{-1}. Based on these related peak intensities at 2140 and 1880 cm^{-1}, Hadjiivanov et al. [44] suggested that oxidation of NO takes place by Fe^{3+} ions which leads to the simultaneous formation of NO^+ (2140 cm^{-1}) and Fe^{2+}-NO species (1880 cm^{-1}). This statement was also supported by Lobree et al. [28], who found mono- and dinitrosyl species on different kinds of iron ions. When ammonia was dosed to NO species adsorbed on Fe-ZSM5, it was clearly discernible from the DRIFT spectra that NH_4^+ ions were generated and that at the same time NO^+ and Fe^{2+}-NO species were consumed, indicated by the disappearance of the characteristic bands at 2140 and 1880 cm^{-1}. However, the standard SCR reaction (1) involves also oxygen, which was found to be responsible for the reoxidation of the catalytic centre during SCR, e.g. over vanadia-based catalysts [33]. It is obvious, that under the oxygen-free conditions in the DRIFT experiment only the first reduction of the iron by NO can take place. The iron remains in the reduced Fe^{2+} state and the catalytic cycle is not closed. These conclusions are corroborated by catalytic tests without oxygen showing only 0–6% $DeNO_x$ from 200 to 450 °C. From investigations of the redox behaviour of Fe-ZSM5, it is known that Fe^{3+} in Fe-ZSM5 is readily reduced to Fe^{2+}, even by simple evacuation at elevated temperatures. However, the reverse process takes place only in oxidizing media [34,35], confirming our conclusions. It should be noted, that in reduced as well as oxidized materials always both forms of iron (Fe^{2+} and Fe^{3+}) are present [34,36] and that oxidation or reduction treatment will just increase or decrease the Fe^{3+}/Fe^{2+} ratio, respectively.

The co-adsorption of NO + O_2 on Fe-ZSM5 (Fig. 4c) produced the same NO^+ and Fe^{2+}-NO species at 2140 and 1880 cm^{-1}, respectively, as observed during adsorption of NO (Fig. 4a). But additional bands were formed at 1635, 1605 and 1578 cm^{-1}, being indicative of adsorbed NO_2 and nitrates. As the same bands were found when NO_2 was adsorbed on Fe-ZSM5 (Fig. 4b), this proves that Fe-ZSM5 is able to oxidize NO to NO_2 and nitrates in the presence of oxygen [37]. When ammonia was passed over NO + O_2 adspecies, again NH_4^+ ions were generated and NO^+ as well as Fe^{2+}-NO species were consumed, but along with the disappearance of the adsorbed NO_2 species at 1635 cm^{-1}, corroborating that both NO and NO_2 are involved in the standard SCR mechanism over Fe-ZSM5. The negligible capacity of H-ZSM5 for the oxidation of NO to NO_2 of only ~1% at $T \leq 350$ °C and ~2% at $T > 350$ °C compared to the high NO_2 yields over Fe-ZSM5, proves the conclusion that the presence of iron in ZSM5 is responsible for the oxidation capacity of NO to NO_2. Our findings are also supported by the results of Long and Yang [38], who performed a different method, i.e. NO_x TPD on H-ZSM5 and Fe-ZSM5.

The observed relation between SCR activity and NO oxidation capability of Fe-ZSM5 and H-ZSM5 furnishes evidence that the negligible SCR activity of H-ZSM5 is due to its low NO oxidizing capability and that the formation of NO_2 is the crucial step in the SCR mechanism on ZSM5 catalysts. The still high catalytic activity of the comparative Fe-ZSM5 sample with only the fortieth part of iron showed that even very low iron contents are sufficient to reach high SCR activities. Therefore, it is likely that iron impurities in H-ZSM5 may be the reason for its residual SCR activity.

The changes in the T–O–T vibration region (800–1000 cm^{-1}) shown in Fig. 5B provide useful information about asymmetric internal stretching vibrations of the zeolite lattice. The bands indicate perturbation by transition metal cations located at exchange sites in zeolites. They shift when the oxidation state of the metal changes or when a substance is adsorbed, which allows us to draw conclusions about the active iron centres during reaction. The disappearance of 1880 cm^{-1} band (Fe^{2+}-NO) and the appearance of the 963 cm^{-1} band, likely caused by T–O–T band perturbations by $[Fe(NH_3)_n]^{2+}$, indicate that Fe is significantly in the 2+ state under reaction conditions. This result was also found under reaction conditions, where the band at 963 cm^{-1} was observed up to 300 °C (Fig. 6B). The generally flat spectrum and the absence of NH_4^+ ion bands at 400 °C is probably caused by very high activity of the catalyst at this temperature (~90% $DeNO_x$ for 1000 ppm NO + 1000 ppm NH_3), i.e. the majority of the ammonia adsorbed on the catalyst reacts too fast at $T \geq 400$ °C to be detected by IR spectroscopy.

The inhibition of the SCR reaction over Fe-ZSM5 by ammonia was observed at lower and intermediate temperatures up to 350 °C. Stevenson et al. [39] who found the same effect on H-ZSM5 suggested that the ammonia inhibition is due to competitive adsorption of NH_3 and NO_x at the active sites with NH_3 dominating at lower temperatures. Based on our results, the inhibition effect for Fe-ZSM5 might be explained by a stronger adsorption of ammonia compared to NO_x on active Fe sites, too. But another explanation is also possible: high SCR activity might be limited to Fe in the 3+ state. The inhibition effect could therefore be explained by an elevated reduction of Fe^{3+} to Fe^{2+} at higher concentrations of NH_3 at $T \leq 300$ °C under SCR conditions. In fact, based on XAFS measurements, Battiston et al. [40] observed an increase in oxidation state of iron from 2.3 to 2.9 after switching from the dosage of SCR reactants to the dosage of only NO in nitrogen at 350 °C. They suggested that the reoxidation might be due to the oxygen traces in the gas phase. Further, Voskoboinikov et al. [41] suggested that the reoxidation of the iron complexes could have been caused by the oxygen from the zeolite matrix. At these high temperatures, Fe^{2+} might be instantaneously re-oxidized in the catalytic cycle.

Since Fe species are responsible for the formation of NO_2, the role of Brønsted or Lewis acid sites is subjected to ammonia storage, which is in line with the observed bands for adsorbed NH_4^+ in the DRIFT experiments. These results are supported by Schraml-Marth et al. [42] as well as Went et al. [43] who also found ammonia to be adsorbed on Brønsted or Lewis acid sites during NH_3 SCR.

5. Conclusions

The iron in Fe-ZSM5 was found to be present in various forms and in various positions. The main role of the iron in NH_3-SCR is to oxidize NO to NO_2, whereas the Brønsted and Lewis acid sites seem to be responsible for binding ammonia on the catalyst surface. The inhibiting effect of ammonia on the SCR activity at lower and intermediate temperatures is attributed to the reduction of Fe^{3+} to $Fe^{2+}$by NH_3.

Acknowledgements

Financial support by the Umicore AG, Germany, is gratefully acknowledged. Pirngruber (Institute for Chemical and Bioengineering, Swiss Federal Institute of Technology, Zurich, Switzerland) and R. Amuthan (CRRP, Swiss Federal Institute of Technology, Lausanne, Switzerland) are kindly acknowledged for carrying out the UV–vis and TEM measurements, respectively.

References

[1] M. Koebel, M. Elsener, M. Kleemann, Catal. Today 59 (2000) 335.
[2] H. Bosch, F. Janssen, Catal. Today 2 (1998) 369.
[3] H.Y. Chen, W.M.H. Sachtler, Catal. Today 42 (1998) 73.
[4] R.Q. Long, R.T. Yang, J. Catal. 188 (1999) 332.
[5] R.Q. Long, R.T. Yang, Catal. Lett. 74 (2001) 201.
[6] F. Heinrich, C. Schmidt, E. Löffler, W. Griinert, Catal. Commun. 2 (2001) 317.
[7] M. Kögel, R. Mönnig, W. Schwieger, A. Tissler, T. Turek, J. Catal. 182 (1999) 470.
[8] M. Devadas, O. Kröcher, A. Wokaun, React. Kinet. Catal. Lett. 86 (2005) 347.
[9] G. Madia, M. Koebel, M. Elsener, A. Wokaun, Ind. Eng. Chem. Res. 41 (2002) 4008.
[10] H.H. Tippins, Phys. Rev. B 1 (1970) 126.
[11] S. Bordiga, R. Buzzoni, F. Geobaldo, C. Lamberti, E. Giamello, A. Zecchina, G. Leofanti, G. Petrini, G. Tozzola, G. Vlaic, J. Catal. 158 (1996) 486.
[12] J. Torrent, V. Barrón, Clays Clay Miner. 51 (2003) 309.
[13] C. Scheinost, A. Chavernas, V. Barron, J. Torrent, Clays Clay Miner. 46 (1998) 528.
[14] G. Centi, F. Vazzana, Catal. Today 53 (1999) 683.
[15] G.D. Pirngruber, M. Luechinger, P.K. Roy, A. Cecchetto, R. Smirniotis, J. Catal. 224 (2004) 429.
[16] A. Brückner, R. Lück, W. Wieker, B. Fahlke, H. Mehner, Zeolites 12 (1992) 380.
[17] D. Goldfarb, M. Bernardo, K.G. Strohmaier, D.E.W. Vaughan, H. Thomann, J. Am. Chem. Soc. 116 (1994) 6344.
[18] M.S. Kumar, M. Schwidder, W. Griinert, A. Brückner, J. Catal. 227 (2004) 384.
[19] H.Y. Chen, El-M. El-Malki, X. Wang, R.A. van Santen, W.M.H. Sachtler, J. Mol. Catal. 162 (2000) 159.
[20] M. Lezcano, V.I. Kovalchuk, J.L. d'ltri, Kinet. Catal. 42 (2001) 104.
[21] G. Mul, J. Pèrez-Ramirez, F. Kapteijn, J.A. Moulijn, Catal. Lett. 80 (2002) 129.
[22] Z.X. Gao, Q. Sun, W.M.H. Sachtler, Appl. Catal. B 33 (2001) 9.
[23] J. Eng, C.H. Bartholomew, J. Catal. 171 (1997) 27.
[24] E.H. Teunissen, R.A. van Santen, A.P.J. Jansen, F.B. van Duijneveldt, J. Phys. Chem. 97 (1993) 203.
[25] N.Y. Topsøe, J. Catal. 128 (1990) 499.
[26] Z. Sobalík, J. Dedecek, I. Ikonnikov, B. Wichterlová, Microporous Mesoporous Mater. 21 (1998) 525.
[27] P. Kubánek, B. Wichterlová, Chem. Listy 96 (2002) 876.

[28] L.J. Lobree, I.-C. Hwang, J.A. Reimer, A.T. Bell, J. Catal. 186 (1999) 242.
[29] H.Y. Chen, T.V. Voskoboinikov, W.M.H. Sachtler, J. Catal. 180 (1998) 171.
[30] L.M. Aparicio, W.K. Hall, Sh. Fang, M.A. Ulla, W.S. Millman, J.A. Dumesic, J. Catal. 108 (1987) 233.
[31] F. Boccuzzi, E. Guglielminotti, F. Pinna, M. Signoretto, J. Chem. Soc., Faraday Trans. 91 (1995) 3237.
[32] S. Yuen, J.E. Kubsh, J.A. Dumesic, N. Topsoee, H. Topsoee, Y. Chen, J. Phys. Chem. 86 (1992) 3022.
[33] M. Koebel, G. Madia, F. Raimondi, A. Wokaun, J. Catal. 209 (2002) 159.
[34] W.K. Hall, X. Feng, J. Dumesic, R. Watwe, Catal. Lett. 52 (1998) 13.
[35] J.O. Petunchi, W.K. Hall, J. Catal. 78 (1982) 327.
[36] L.M. Aparicio, J.A. Dumesic, S.-M. Fang, M.A. Long, M.A. Ulla, W.S. Millman, W.K. Hall, J. Catal. 104 (1987) 381.
[37] L.J. Lobree, I.-C. Hwang, A. Reimer, A.T. Bell, Catal. Lett. 63 (1999) 233.
[38] R.Q. Long, R.T. Yang, J. Catal. 198 (2001) 20.
[39] S.A. Stevenson, J.C. Vartuli, C.F. Brooks, J. Catal. 190 (2000) 228.
[40] A.A. Battiston, J.H. Bitter, D.C. Koningsberger, J. Catal. 218 (2003) 163.
[41] T.V. Voskoboinikov, H.-Y. Chen, W.M.H. Sachtler, Appl. Catal. B 19 (1998) 279.
[42] M. Schraml-Marth, A. Wokaun, A. Baiker, J. Catal. 124 (1990) 86.
[43] G.T. Went, L.-J. Leu, R.R. Rosin, A.T. Bell, J. Catal. 134 (1992) 492.
[44] K. Hadjiivanov, H. Knözinger, B. Tsyntsarski, L. Dimitrov, Catal. Lett. 62 (1999) 35.